THE ROYAL SOCIETY

doi 10.1098/rspb.2001.1829

A new approach to analysing texture-defined motion

Christopher P. Benton[1]* **and Alan Johnston**[2]

[1]*Department of Experimental Psychology, University of Bristol, 8 Woodland Road, Bristol BS8 1TN, UK*
[2]*Department of Psychology, University College London, Gower Street, London WC1E 6BT, UK*

It has been widely accepted that standard low-level computational approaches to motion processing cannot extract texture-defined motion without applying some pre-processing nonlinearity. This has motivated accounts of motion perception in which luminance- and texture-defined motion are processed by separate mechanisms. Here, we introduce a novel method of image description where motion sequences may be described in terms of their local spatial and temporal gradients. This allows us to assess the local velocity information available to standard low-level motion mechanisms. Our analysis of several texture–motion stimuli shows that the information indicating correct texture–motion velocity and/or direction is present in the raw luminance measures. This raises the possibility that luminance–motion and texture–motion may be processed by the same cortical mechanisms. Our analysis offers a way of looking at texture–motion processing that is, to our knowledge, new and original.

Keywords: vision; motion; neurophysiology; second order; non-Fourier; texture

1. INTRODUCTION

The images falling across our retinas are spatio-temporally structured. In order to extract information from this shifting optic array our visual system must be sensitive not only to spatial patterns, but also to temporal change. It has long been established that simple and complex cells in the primary visual cortex of the cat and monkey exhibit directional selectivity (Hubel & Wiesel 1962, 1968). Similar mechanisms are thought to underlie human motion perception. Computational models of motion processing attempt to both describe the algorithms through which motion may be computed in biological systems and account for the motion-selective responses of cortical neurons.

Computational models of low-level motion processing are based on the notion that simple neural processes respond directly to changes in local image luminance. Image motion is extracted through a nonlinear combination of the outputs of linear filters (Adelson & Bergen 1985; Van Santen & Sperling 1985; Watson & Ahumada 1985; Johnston *et al*. 1992). Such models drive a great deal of neurophysiological and psychophysical research. These models are designed to operate on stimuli in which motion is defined by translations of luminance. For the present purposes we therefore define such models as being 'luminance based'. Stimulus motion in texture-defined motion stimuli is defined not by translations of luminance but by translations of some other texture property such as contrast or spatial frequency. Some examples of texture-defined motion may be readily perceived by human observers, yet, it is widely believed, cannot readily be analysed by luminance-based motion models (Chubb & Sperling 1988; Cavanagh & Mather 1989; Benton & Johnston 1997).

In order to account for the perception of texture-defined motion it has been proposed that some process (or processes) other than standard low-level motion analysis must operate (Chubb & Sperling 1989). The mechanisms proposed fall into two groups. In the first, the input image is subject to some gross nonlinearity prior to standard motion analysis. The effect of this nonlinear pre-processing is effectively to translate texture motion into luminance motion so that it becomes accessible to standard motion analysis (Chubb & Sperling 1988). In the second, some high-level feature tracking mechanism is applied to the stimulus (Cavanagh 1992). Whilst the latter has a long history within the field of motion perception, there is no general agreement as to what specifies a feature, what mechanism may be applied to tracking the motion of those features or how object speed is determined. At its simplest level, feature tracking may simply represent awareness of a positional change in attentional focus.

The central motivation for the proposal that some process other than standard low-level motion analysis must operate is the belief that mechanisms of this type cannot analyse texture-defined motion. Here, we present what is, to our knowledge, a novel analysis of some texture-defined motion stimuli. We demonstrate that the information for the direction and speed of motion in a number of texture–motion stimuli is directly available to standard low-level motion analysis. We challenge the widely held belief that texture-defined motion cannot be detected by luminance-based motion mechanisms. Our analysis offers a new perspective on the manner in which texture–motion may be processed.

2. METHODS

The local velocity in an image can be calculated by taking the ratio of the local temporal gradient to the local spatial gradient (Fennema & Thompson 1979; Horn & Schunck 1981; Sobey & Srinivasan 1991; Johnston *et al*. 1992; Verri *et al*. 1992). These measures may be presented in the form of a gradient plot in which we show the distribution of points that have a particular spatial and temporal gradient. This novel method of image analysis allows us to investigate the distribution of local

*Author for correspondence (chris.benton@bristol.ac.uk.).

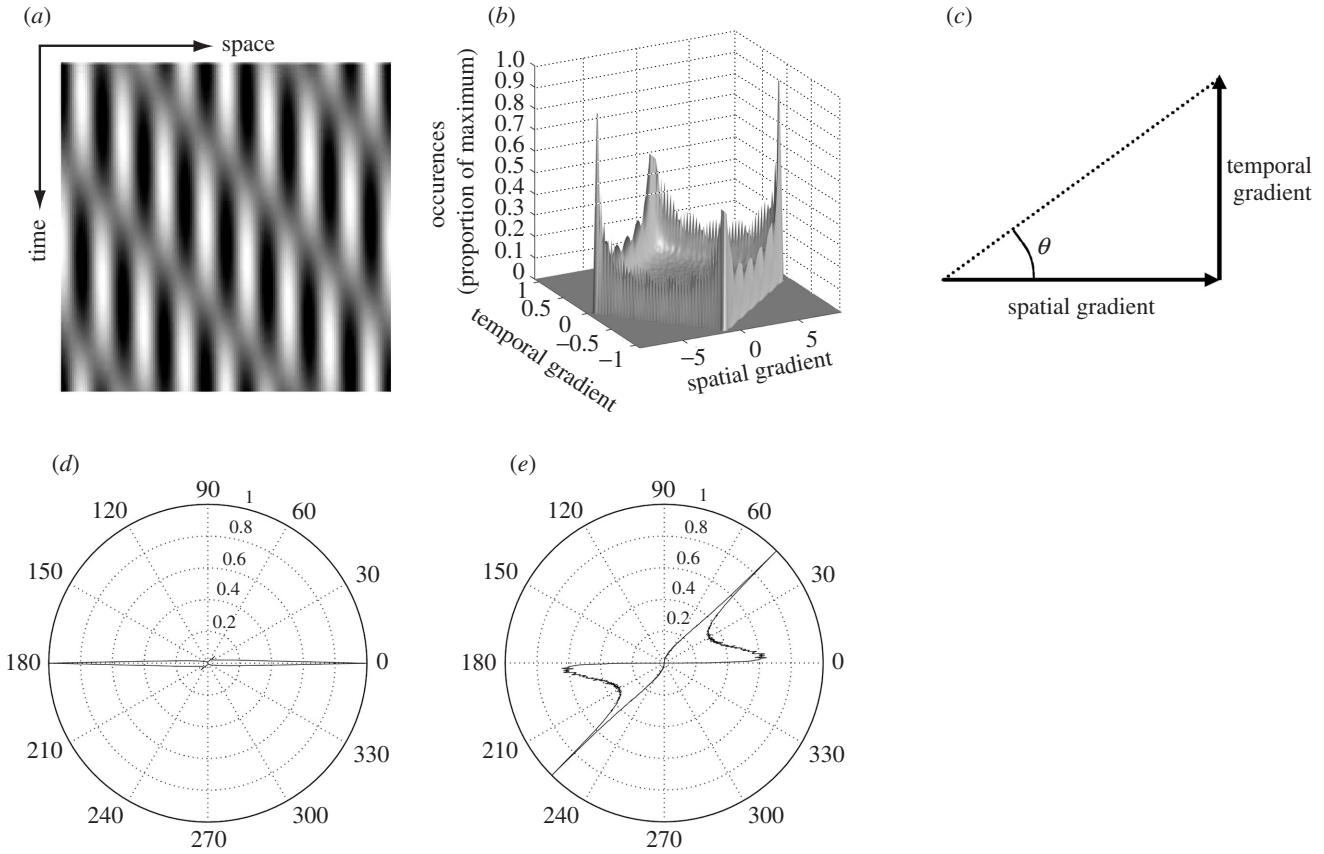

Figure 1. (*a*) Space–time plot of the beat pattern. (*b*) Gradient plot of the beat pattern. (*c*) Relationship between spatial and temporal gradients expressed as an angle. (*d*) Number of occurrences of each angle for the beat stimulus. The maximum value is normalized to unity. (*e*) Residual 'velocity' plot (more accurately a plot of residual velocities expressed as angles) of the beat stimulus.

image velocities occurring within an image. Lines through the origin of a gradient plot are lines of iso-velocity where velocity is given by the tangent of the angle between the line and the spatial gradient axis. The distance of a point from the origin reflects the magnitude of the spatio-temporal gradient.

All space–time input images measured 256 pixels × 256 pixels, with space represented horizontally and time represented vertically. For ease of description, we arbitrarily assign 256 pixels across to a width of 1° and 256 pixels down to a temporal extent of 1 s. Two of the stimuli that we examine, beats and contrast-modulated sine waves, are described by continuous functions that can be readily differentiated at any point in the image. For these, we randomly sample the function defining the stimulus at 10 million points and extract the temporal and spatial gradients by calculating the partial derivatives at each of these points. From each point that we sample, we obtain a temporal gradient and a spatial gradient. The full range of spatial and temporal gradients obtained is divided into 100 bins × 100 bins, with each bin signifying a small range of spatio-temporal gradients. Each spatial gradient/temporal gradient pair is then assigned to its relevant bin in order to obtain a plot of the number of occurrences per bin. Note that these have been normalized to a maximum of unity.

A less formal description runs as follows. Temporal gradient/spatial gradient pairs can be plotted on a graph with the spatial gradient on the horizontal axis and the temporal gradient on the vertical axis. However, the scatter plot resulting from plotting all of the gradient pair samples from an image would be unclear because of the large number of samples that we use. In some areas, points would overlap or lie on top of one another such that the scatter plot would not give a valid representation of the frequency of occurrence of certain gradient pairs. In order to create our gradient plot we divide the scatter plot into a grid and count the number of gradient pairs falling into each rectangle of the grid. We then plot this as a histogram so that the height of each bar represents the number of instances of gradient pairs falling into each of the rectangles into which the scatter plot is divided.

The other stimuli examined in this paper involve manipulations of binary noise. With these, we cannot differentiate the function analytically. In order to extract the gradient present in the image we use the observation that filtering a differentiated image with a filter kernel is equivalent to filtering the undifferentiated image with the differentiated filter kernel (Bracewell 1965). This observation forms the basis of models that seek to measure the local image velocity using gradient techniques. In order to measure spatial gradients we apply a filter that is Gaussian temporally and the first derivative of a Gaussian spatially, whereas for extracting temporal gradients our filter is a Gaussian spatially and the first-order derivative of a Gaussian temporally. The standard deviation along both dimensions is 2 pixels (0.47 arcmin and 7.8 ms) in each filter function. Because these images use a random carrier, we gather results over 200 images, which thereby gives us a total of over 10 million measures of spatial and temporal gradients. We then apply the same analysis as that applied to the beat pattern.

3. RESULTS

(a) *Translating beat pattern*

A static high-frequency sine wave (the carrier) is multiplied by a translating lower-frequency sinusoid. An example is shown in figure 1*a*. The envelope spatial frequency for this and all other stimuli was 1 cycle deg^{-1} and the carrier spatial frequency was 8 cycles deg^{-1}. The envelope temporal frequency was 1 Hz in the example shown in figure 1. The stimulus is characterized by its translating grey regions (moving from left to right in the example shown) and by the contrast reversal in the underlying static carrier. Figure 1*b* shows this image expressed in terms of a gradient plot. One can readily see that there are four peaks in gradient space, a pattern we have found to be characteristic of beat patterns. Note the difference in scale between the axes showing the spatial and temporal gradients. This makes it difficult to obtain a true idea of the velocity as indicated by the orientation of the peaks in relation to the origin.

We are faced with the issue of how to extract the velocities signalled by the dominant features in our gradient plots. The simplest analysis that we could apply to our gradient data from the beat pattern would be to identify the positions of the peaks. Unfortunately this procedure cannot be applied to all of the gradient plots that we examine in this study. This is because the dominant features within the gradient plots are not necessarily well-defined peaks lying at some distance from the origin of the gradient plot. In order to extract the velocity we use a procedure in which we create a residual velocity plot from the velocity information in the gradient data and then identify peaks in the residual velocity plot. This gives us a simple computational procedure with which to extract velocity information from our plots. It should be emphasized that we are not proposing that this procedure be implemented biologically. It is simply a method of analysis that appears to pick out the velocities signalled by the dominant features in the velocity plots that we have examined.

Since velocity is the ratio of the temporal gradient to the spatial gradient, points indicating a particular velocity will fall on a line through the origin at some angle θ to the spatial gradient axis. We express each local combination of spatial and temporal gradients as an angle, as shown in figure 1*c*. These samples are gathered into bins of 0.25°. The resultant data are plotted in polar form in figure 1*d*. Plotting the data in this form gives us another way of visualizing the local velocities present in the image (as velocity is given by the tangent of the angle). The distance from the centre indicates the number of occurrences per bin. It can be readily seen from figure 1*d* that this plot is dominated by the static information in the image, which is signified by angles of 0 and 180°. This is due to the influence of the static carrier with the image.

However, we are most interested in any residual velocities present in the image. In order to calculate these we take the difference between the numbers of points signalling the same speed, but in opposite directions. In the velocity plot, angles of θ and $\theta+\pi$ correspond to the same velocity (v), whilst angles of $-\theta$ and $-\theta+\pi$ correspond to a velocity of $-v$ (since a reversal in direction is accompanied by a change in the sign of either the temporal or the spatial gradient). If N_θ is the number of instances of gradient combinations falling into a bin centred around θ in the velocity plot then the residual velocity at angle θ can be calculated as

$$R_\theta = R_{\theta+\pi} = (N_\theta + N_{\theta+\pi}) - (N_{-\theta} + N_{-\theta+\pi}). \tag{3.1}$$

We plot only positive values of R_h for our residual velocity plot because

$$R_{-\theta} = R_{-\theta+\pi} = -R_\theta = -R_{\theta+\pi}. \tag{3.2}$$

In other words, setting negative values to zero results in no loss of information. The only two places where this procedure of letting opposite velocities cancel one another out is invalid are where velocity is zero ($\theta=0$ and $\theta=\pi$) and where velocity is infinite ($\theta=\pi/2$ and $\theta=3\pi/2$). At these points we calculate the following:

$$R_0 = R_\pi = |N_0 - N_\pi| \tag{3.3}$$

and

$$R_{\pi/2} = R_{3\pi/2} = |N_{\pi/2} - N_{3\pi/2}|. \tag{3.4}$$

In practice, this allows instances of zero and infinite velocities in the velocity plot to cancel one another out in the residual velocity plot.

The results from these calculations are shown in figure 1*e*. The residual velocity plot is a measure of what is left when opposite velocities have been subtracted from one another. Note that, as a result of our procedure, the data are symmetrical, such that the number of occurrences at any angle θ is identical to the number of occurrences at

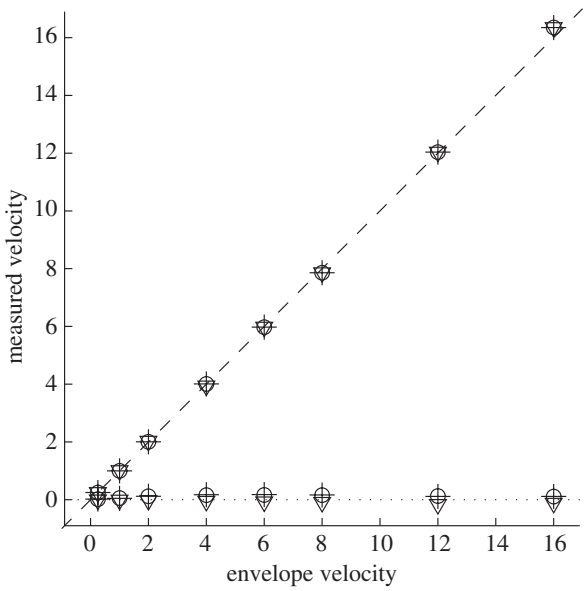

Figure 2. Velocities from peaks identified in residual velocity plots for three stimuli as a function of the envelope velocity. Circles show the results for the beat pattern (figure 1*a*), crosses show the results for a contrast-modulated sine wave (figure 3*a*) and inverted triangles show the results for a contrast-modulated noise stimulus (figure 4*a*). Note that, in many cases, the close overlap between the stimuli makes identification difficult. The horizontal dotted line shows the carrier velocity and the dashed diagonal line shows the envelope velocity.

$\theta + 180°$. From figure 1*e*, we obtain peaks in this distribution at 45° and at a value of just greater than 0°. We identify these two peaks in the data and express them as a velocity. These measures are plotted as a function of the envelope velocity in figure 2. The diagonal line indicates the veridical envelope velocity and the horizontal line indicates a speed of zero. As one can see from the plot, the peaks in our velocity data reliably indicate the velocity of the envelope motion and a velocity of close to zero, corresponding to the static carrier.

With the beat pattern, this method of analysis essentially picks out the peaks shown in the gradient plot in figure 1*b*. These peaks can be divided into pairs where one peak indicates the velocity of the envelope and the other peak indicates the velocity of the carrier. A simple peak-finding algorithm applied to the data in figure 1*b* confirms the findings shown in figure 2. The data show that information about the envelope velocity is present in this local analysis of the space–time image. From the gradient plot in figure 1*b* it is clear that the peaks indicating envelope and carrier motion dominate the plot.

Note that the velocity close to zero that we identify as corresponding to the carrier velocity actually indicates forward motion. However, a peak-finding algorithm applied to the gradient plot finds this velocity to be zero. The reason for the discrepancy is that our procedure for creating residual velocity plots allows velocities of zero to cancel one another. Note also that any actual model will use filtering operations that will, in all likelihood, change the balance of components within the stimuli. A beat stimulus is constructed by adding two sine waves of equal amplitude. When passed through some filter (such as a Gaussian in space and time), it is likely that one sine wave will be attenuated relative to another. This will clearly change the characteristics of the stimulus and can potentially introduce luminance-defined motion with a direction opposite to that of the texture-defined motion. Our analysis shows the information that is available in the ideal case from a simple gradient-based analysis.

(b) *Contrast-modulated sine wave*

In this stimulus a static sinusoidal carrier is multiplied by a raised sine wave (see figure 3*a*). The method of analysis for the contrast-modulated sine wave is identical to that for the beat pattern. However, in this case we obtain a quite different pattern in the gradient plot, finding a large orientated central peak (see figure 3*b*). When we apply our analysis we arrive at a residual velocity plot that is very similar to that found with the beat pattern (figure 3*c*). As one can see from the measured velocity plotted as a function of the envelope velocity shown in figure 2, our analysis again picks out the envelope velocity and a velocity close to zero. With this particular stimulus, our analysis serves to pick out the orientation of the central spiked feature that dominates the gradient plot. The orientation of this feature gives the correct envelope velocity.

(c) *Contrast-modulated static noise*

This stimulus is similar to the contrast-modulated sine wave except that we use a static binary noise carrier. The noise has a width of 4 pixels. There is no spatial modulation within noise elements. A space–time plot of the stimulus is shown in figure 4*a*. Stimuli of this type (which are referred to as micro-balanced) have been shown to be particularly problematic for directionally selective luminance-based motion models (Chubb & Sperling 1988; Benton & Johnston 1997).

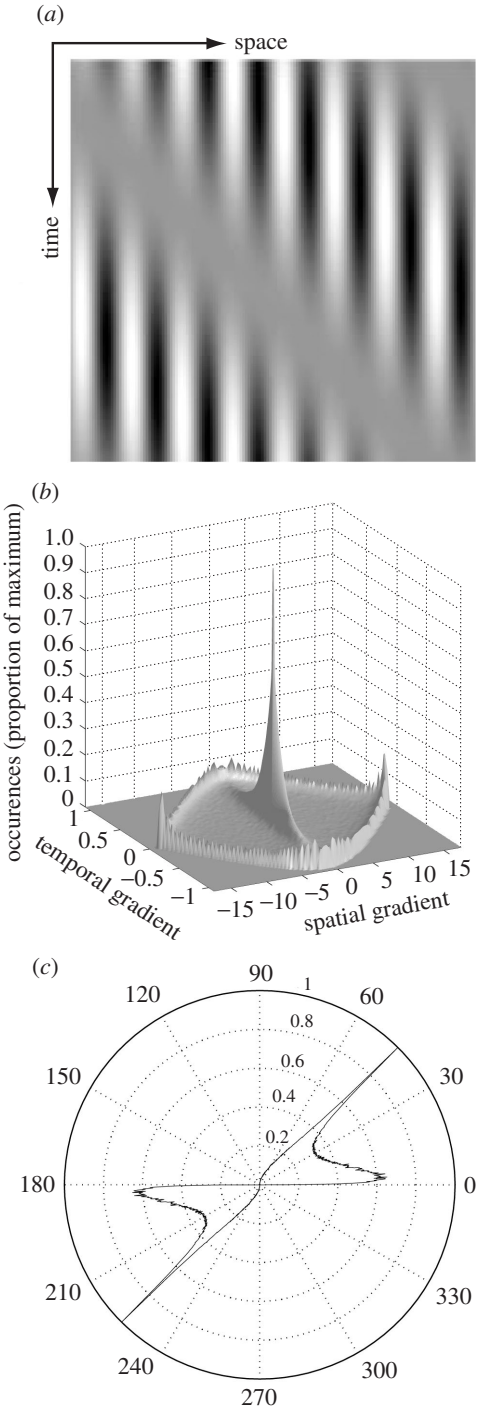

Figure 3. (*a*) Space–time plot of a contrast-modulated sine wave. (*b*) Gradient plot of a contrast-modulated sine wave. (*c*) Residual velocity plot (expressed in angular form) of a contrast-modulated sine wave.

Figure 4*b* shows a gradient plot of the stimulus. The three peaks shown in the plot form part of an orientated feature that lies on the line through gradient space describing the velocity of the envelope (as confirmed by a peak-finding algorithm). Our residual velocity plot, which is shown in figure 4*c*, clearly picks out the orientation of

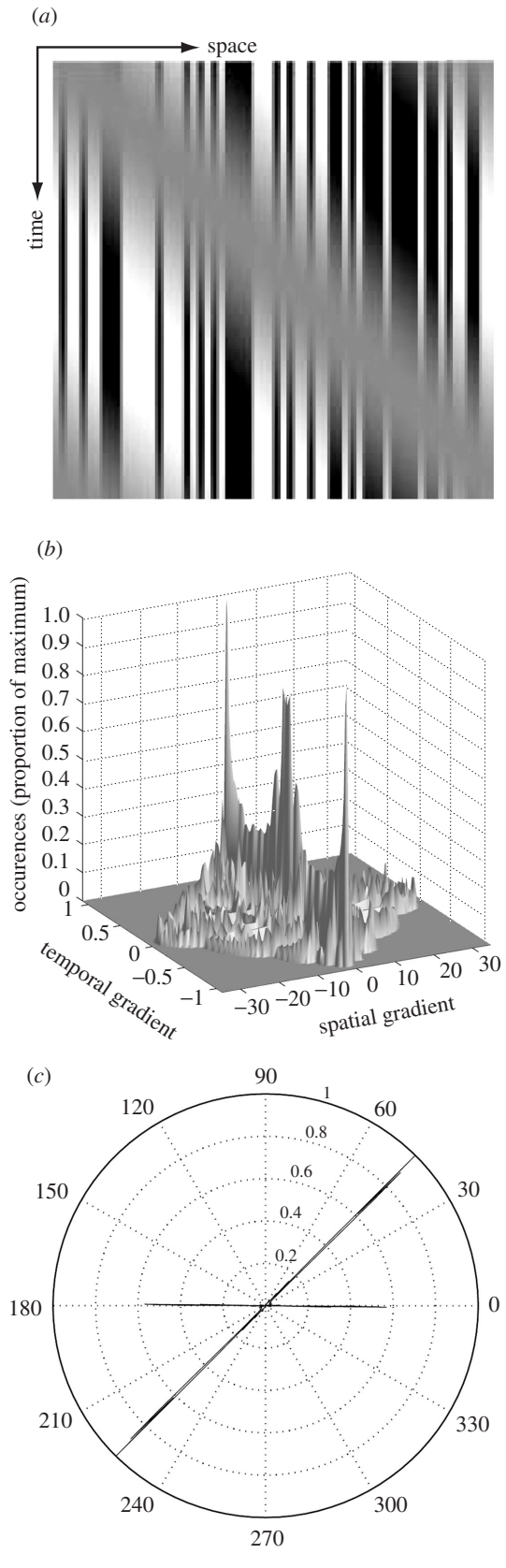

Figure 4. (*a*) Space–time plot of a contrast-modulated static noise pattern. (*b*) Gradient plot of a contrast-modulated static noise. (*c*) Residual velocity plot of a contrast-modulated static noise stimulus.

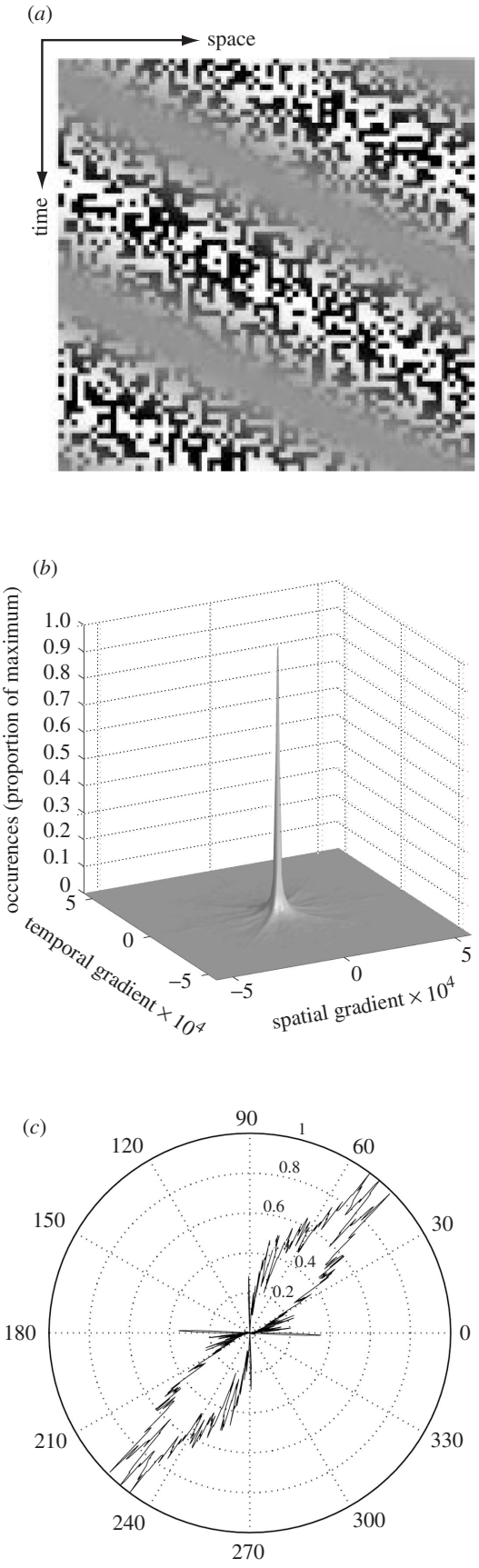

Figure 5. (*a*) Space–time plot of a contrast-modulated dynamic noise pattern. (*b*) Gradient plot of a contrast-modulated dynamic noise. (*c*) Residual velocity plot of a contrast-modulated dynamic noise stimulus.

Table 1. Percentages of local velocity measures falling between specified limits for beats and various contrast modulations.

(The envelope velocity was $1^\circ s^{-1}$. The carrier characteristics are as specified in § 3.)

	beat	contrast-modulated sine wave	contrast-modulated static noise	contrast-modulated dynamic noise
$0.9 \leqslant v < 1.1$	2.7	2.5	12.7	6.0
$-0.1 \leqslant v < 0.1$	45.6	45.6	48.8	7.3
$0.0 < v$	57.8	57.8	59.1	53.0

this feature in gradient space and, when we plot the peak residual velocities in this image (figure 2), we can again show that the envelope velocity is present in this image.

(d) ***Contrast-modulated dynamic noise***

A sinusoidal envelope modulates the contrast of a dynamic noise carrier. In the example shown in figure 5 the envelope velocity is $2^\circ s^{-1}$. There is no spatial or temporal modulation within the noise elements, that measure 4 pixels × 4 pixels. In terms of its gradient, this stimulus has a central orientated spike (figure 5*b*). The analysis of residual velocity gives us the correct direction of motion in this stimulus (figure 5*c*). However, the residual velocity plot is very noisy and the correct envelope velocity was not readily obtained. It may be that the use of the first derivatives is insufficient for extracting the envelope velocity and that additional measures need to be taken (Johnston *et al*. 1992, 1999*a*,*b*; Benton *et al*. 2000).

We have chosen the method of analysis described because it picks out what appear to be dominant features in each of the respective gradient plots. This shows that the information that can give the velocity and/or direction of envelope motion to luminance-based mechanisms is present in the stimuli. It can also be shown that this approach can recover the direction of motion of the flicker rate of dynamic noise and the noise check size in sinusoidal modulations. For example, this can be accomplished by applying band pass filters to the space–time image prior to gradient analysis. In essence this converts the images into contrast modulations.

4. DISCUSSION

We analysed the local image velocities present in a number of image sequences in which motion was defined by the translation of texture contrast. Our results unambiguously demonstrate that, with some texture-defined motion stimuli, information that allows the velocity of texture-defined motion to be extracted by a luminance-based motion mechanism exists within the stimulus. If this information is used as part of the process of motion perception, then luminance- and texture-defined motion could be processed by the same cortical mechanisms.

We can write any contrast modulation stimulus $f(x,t)$ as the product of two functions, namely an envelope $g(x,t)$ and a carrier $h(x,t)$. The velocity v is given by the ratio of the temporal derivative to the spatial derivative, i.e.

$$v = \frac{f_t(x,t)}{f_x(x,t)} = \frac{g_t(x,t)h(x,t) + g(x,t)h_t(x,t)}{g_x(x,t)h(x,t) + g(x,t)h_x(x,t)}, \tag{4.1}$$

where a subscript t indicates temporal differentiation and a subscript x indicates spatial differentiation. When $g(x,t)$ is close to zero and/or both $h_t(x,t)$ and $h_x(x,t)$ are close to zero then

$$v \approx \frac{g_t(x,t)}{g_x(x,t)}. \tag{4.2}$$

In other words, when the contrast is close to zero or when both the temporal and spatial derivatives of the carrier are close to zero then the calculated velocity will be close to that of the envelope. We should therefore fully expect that local velocities close to the speed of the envelope should be present in our gradient-based image analyses.

The belief that texture-defined motion cannot be recovered without recourse to some nonlinearity prior to motion processing is deeply embedded within the literature. Our analysis shows that the information for the direction of motion and/or the velocity of texture-defined motion may be accessed by luminance-based mechanisms without recourse to pre-processing nonlinearities. In the stimuli that we describe, gradient combinations signalling luminance–motion form a substantial proportion of the total number of residual velocity measures. We have shown that gradient-based computational models of biological motion processing can successfully recover texture-defined motion in a number of studies (Johnston *et al*. 1992, 1999*a*; Johnston & Clifford 1995*a*; Benton *et al*. 2000, 2001). Our analysis here shows that there is information present in some second-order motion sequences that is directly accessible to a generic gradient-based approach.

The gradient combinations signalling the envelope velocity in the beat and contrast-modulated sine wave stimuli form only a small proportion of the total number of measures (see table 1). A large proportion of the measures signal velocities that lie close to zero. Our analysis does show that gradient combinations giving velocities close to that of the envelope do predominate in the residual velocity plot (particularly if velocities close to zero are ignored). In order to account for the perception of envelope motion based upon these measures one would have to propose the existence of mechanisms capable of analysing and organizing local velocity measures. However, it may well be the case that an approach in which multiple gradient measures are combined can detect the envelope velocity in stimuli of this type correctly. Johnston & Clifford (1995*a*) investigated contrast-modulated sine waves using a computational model in which multiple gradient measures are combined in order to arrive at local velocity estimates. They found a

close match between psychophysical measures of envelope velocity and the velocity derived from the model output. Interestingly, the model correctly predicted the non-veridical velocity perceived when subjects viewed a translating contrast modulation of a translating sinusoidal carrier.

In the gradient approach upon which our analysis is based, velocity is extracted by taking the ratio of the temporal and spatial derivatives. This is, of course, a nonlinear operation. Nonlinear operations are employed in all major approaches to low-level motion perception (Reichardt 1961; Van Santen & Sperling 1984, 1985; Adelson & Bergen 1985, 1986; Johnston *et al*. 1992*b*). These nonlinearities form an integral part of the various motion extraction algorithms. The crucial point here, at least in terms of gradient-based approaches, is that those nonlinearities that are an intrinsic part of the motion algorithm may be sufficient for extracting texture-defined motion.

The analysis that we have described should not be taken as a biological model of motion processing. We simply identify the information that is available from first-order image derivatives. Computational approaches that use this information may potentially recover the direction of motion or velocity from some texture–motion stimuli. It is likely that any model that realistically attempts to account for the biological computation of motion would include additional measures or calculations to those described here (Adelson & Bergen 1986; Johnston *et al*. 1992, 1999*b*; Johnston & Clifford 1995*b*; Benton *et al*. 2000). It is not necessarily the case that any model that uses these measures will return a veridical envelope velocity (Johnston & Clifford 1995*a*). Whilst our analysis of local first-order gradients does show that velocity can be recovered in some texture–motion stimuli, we only find the correct direction but not the correct speed with contrast modulations of dynamic noise. It may well be the case that we have simply not identified the correct measures needed for extracting velocity in stimuli of this type. In addition, it is possible that some portion of the perception of texture-defined motion is accounted for by a high-level feature tracking mechanism (Seiffert & Cavanagh 1998, 1999; Derrington & Ukkonen 1999; Ukkonen & Derrington 2000).

When all Fourier components of a pattern travel at the same velocity, all spatial gradient/temporal gradient combinations must fall on a single line through the origin of the gradient plot. In this case, the correct extraction of stimulus direction and/or motion can potentially result from a measure taken from any spatio-temporal location within the image. In the case of our texture-defined motion sequences, it is clear that there is a large range of gradient-based velocities present in the image and that these may signal motion of various speeds and in opposing directions. If the perception of texture-defined motion is based upon these local luminance measures then mechanisms capable of resolving complex motion fields may well play a part in the detection of texture–motion.

Plant & Nakayama (1993) and Plant *et al*. (1993) described results across three patients with unilateral lesions of the extrastriate cortex. Their subjects showed a deficit for detection of the direction of motion with texture–motion stimuli. Damage to extrastriate area MT is believed to cause impaired performance on luminance–motion stimuli with noisy velocity fields (Baker *et al*. 1991). As we have shown, in our gradient-based analysis the local velocities describing texture–motion are accompanied by many other local velocities. The problem of extracting the dominant texture–motion is akin to that of extracting the dominant luminance–motion from a noisy velocity field. One might therefore expect that damage to area MT resulting in performance deficits for noisy luminance-defined motion should also produce deficits in direction discrimination for texture-defined motion.

The three patients with extrastriate damage described by Plant & Nakayama (1993) and Plant *et al*. (1993) also showed deficits in velocity discrimination with luminance-defined motion stimuli. It has been proposed that extrastriate area MT plays a part in velocity coding (Heeger *et al*. 1996; Simoncelli & Heeger 1998). Given that Plant & Nakayama (1993) and Plant *et al*. (1993) proposed that the lesions of their subjects may include human MT, a deficit in velocity discrimination might well be expected. We cannot yet tell whether damage to the same mechanism is responsible for both the direction discrimination deficit with texture–motion and the velocity discrimination deficit with luminance–motion. It is possible that the resolution of complex velocity fields and the extraction of stimulus velocity both require similar integrative processes.

The notion that both luminance- and texture-defined motion are both processed by the same mechanisms clearly sits well with those studies that have obtained no strong evidence for a difference in the locality of cortical processing between the two types of stimulus (Victor & Conte 1992; Patzwahl *et al*. 1994; Greenlee & Smith 1997; Braun *et al*. 1998; Smith *et al*. 1998; Somers *et al*. 1998, 1999). The pattern of results seen in two patients studied by Vaina & Cowey (1996) and Vaina *et al*. (1998, 1999) is however somewhat problematic for our analysis. Patient F. D. showed a deficit in texture–direction discrimination whilst showing no luminance–motion deficits. Patient R. A. showed a deficit with luminance-defined motion but not with texture-defined motion. These findings have been taken as evidence for a double dissociation between luminance–motion and texture–motion processing. The fact that a large number of other studies using a variety of techniques have failed to locate different processing regions for luminance- and texture-defined motion should be some cause for concern. There is a clear difference in the types of stimuli employed by Vaina & Cowey (1996) and Vaina *et al*. (1998, 1999) and those employed by other researchers. The vast majority of studies have used simple texture–motion sequences, such as beat patterns and sinusoidal contrast modulations. Vaina & Cowey (1996) and Vaina *et al*. (1998, 1999) employed a rather complex set of luminance–motion and texture–motion sequences, many of which either contained a considerable dynamic noise content or required some integrative process after low-level motion extraction (i.e. they are global motion stimuli). A better test would be to use simple stimuli where there can be less chance of interaction between complex stimulus attributes and the type of motion stimulus. This might allow us to resolve the discrepancies that exist between the data from Vaina & Cowey (1996) and Vaina *et al*. (1998, 1999) and other researchers in the field.

Our approach offers a theoretical alternative to the standard computational approach to the detection of luminance-defined motion in which the signal is subject to some nonlinearity prior to motion analysis. It offers an account in which the detection of luminance-defined motion can occur simply as a by-product of the normal process of motion analysis. Our suggestion that some texture-defined motion can be detected through the operation of luminance-based mechanisms should not be taken to mean that no additional motion processes operate. There is good evidence for high-level feature tracking in human motion perception (Cavanagh 1992; Lu & Sperling 1995), and such a process could potentially play a part in the perception of texture-defined motion.

REFERENCES

Adelson, E. H. & Bergen, J. R. 1985 Spatiotemporal energy models for the perception of motion. *J. Opt. Soc. Am.* A **2**, 284–299.

Adelson, E. H. & Bergen, J. R. 1986 The extraction of spatio-temporal energy in human and machine vision. In *Proceedings—workshop on motion: representation and analysis* (ed. T. Huang & J. Tsotsos), pp. 151–156. Charleston, SC: Institute of Electrical and Electronics Engineers, Comp Soc.

Benton, C. & Johnston, A. 1997 First-order motion from contrast modulated noise? *Vis. Res.* **37**, 3073–3078.

Benton, C. P., Johnston, A. & McOwan, P. W. 2000 Computational modelling of interleaved first- and second-order motion sequences and translating $3f+4f$ beat patterns. *Vis. Res.* **40**, 1135–1142.

Benton, C. P., Johnston, A., McOwan, P. W. & Victor, J. D. 2001 Computational modelling of non-Fourier motion: further evidence for a single luminance-based mechanism. *J. Opt. Soc. Am.* A **18**, 2204–2208.

Bracewell, R. N. 1965 *The Fourier transform and its applications*. New York: McGraw-Hill.

Braun, D., Petersen, D., Schönle, P. & Fahle, M. 1998 Deficits and recovery of first- and second-order motion perception in patients with unilateral cortical lesions. *Euro. J. Neurosci.* **10**, 2117–2128.

Cavanagh, P. 1992 Attention-based motion perception. *Science* **257**, 1563–1565.

Cavanagh, P. & Mather, G. 1989 Motion: the long and the short of it. *Spat. Vis.* **4**, 103–129.

Chubb, C. & Sperling, G. 1988 Drift-balanced random dot stimuli: a general basis for studying non-Fourier motion perception. *J. Opt. Soc. Am.* A **5**, 1986–2007.

Chubb, C. & Sperling, G. 1989 Two motion perception mechanisms revealed through distance-driven reversal of apparent motion. *Proc. Natl Acad. Sci. USA* **86**, 2985–2989.

Derrington, A. M. & Ukkonen, O. I. 1999 Second-order motion discrimination by feature-tracking. *Vis. Res.* **39**, 1465–1475.

Fennema, C. L. & Thompson, W. B. 1979 Velocity determination in scenes containing several moving objects. *Comp. Graphics Image Process.* **9**, 301–315.

Greenlee, M. W. & Smith, A. T. 1997 Detection and discrimination of first- and second-order motion in patients with unilateral brain damage. *J. Neurosci.* **17**, 804–818.

Heeger, D. J., Simoncelli, E. P. & Movshon, J. A. 1996 Computational models of cortical visual processing. *Proc. Natl. Acad. Sci. USA* **93**, 623–627.

Horn, B. K. P. & Schunck, B. G. 1981 Determining optical flow. *Artif. Intel.* **17**, 185–203.

Hubel, D. & Wiesel, T. 1962 Receptive fields, binocular interaction and functional architecture in the cat's visual cortex. *J. Physiol. Lond.* **160**, 106–154.

Hubel, D. H. & Wiesel, T. N. 1968 Receptive fields and functional architecture of monkey striate cortex. *J. Physiol.* **195**, 215–243.

Johnston, A. & Clifford, C. W. G. 1995*a* Perceived motion of contrast modulated gratings: predictions of the multi-channel gradient model and the role of full-wave rectification. *Vis. Res.* **35**, 1771–1783.

Johnston, A. & Clifford, C. W. G. 1995*b* A unified account of three apparent motion illusions. *Vis. Res.* **35**, 1109–1123.

Johnston, A., McOwan, P. W. & Buxton, H. 1992 A computational model of the analysis of some first-order and second-order motion patterns by simple and complex cells. *Proc. R. Soc. Lond.* B **250**, 297–306.

Johnston, A., Benton, C. P. & McOwan, P. W. 1999*a* Induced motion at texture-defined motion boundaries. *Proc. R. Soc. Lond.* B **266**, 2441–2459. (DOI 10.1098/rspb.1999.0944.)

Johnston, A., McOwan, P. W. & Benton, C. P. 1999*b* Robust velocity computation from a biologically motivated model of motion perception. *Proc. R. Soc. Lond.* B **266**, 509–518. (DOI 10.1098/rspb.1999.0666.)

Lu, Z.-L. & Sperling, G. 1995 Attention-generated apparent motion. *Nature* **377**, 237–239.

Patzwahl, D. R., Zanker, J. M. & Altenmüller, E. O. 1994 Cortical potentials reflecting motion processing in humans. *Vis. Neurosci.* **11**, 1135–1147.

Plant, G. T. & Nakayama, K. 1993 The characterisitics of residual motion perception in the hemifield contralateral to lateral occipital lesions in humans. *Brain* **116**, 1337–1353.

Plant, G. T., Laxer, K. D., Barbaro, N. M., Schiffman, J. S. & Nakayama, K. 1993 Impaired visual motion perception in the contralateral hemifield following unilateral posterior cerebral lesions in humans. *Brain* **116**, 1303–1335.

Reichardt, W. 1961 Autocorrelation, a principle for the evaluation of sensory information by the central nervous system. In *Sensory communication* (ed. W. A. Rosenblith), pp. 303–317. New York: Wiley.

Seiffert, A. E. & Cavanagh, P. 1998 Position displacement, not velocity, is the cue to motion detection of second-order stimuli. *Vis. Res.* **38**, 3569–3582.

Seiffert, A. E. & Cavanagh, P. 1999 Position-based motion perception for color and texture stimuli: effects of contrast and speed. *Vis. Res.* **39**, 4172–4185.

Simoncelli, E. P. & Heeger, D. J. 1998 A model of neuronal responses in visual area MT. *Vision Res.* **38**, 743–762.

Smith, A. T., Greenlee, M. W., Singh, K. D., Kraemer, F. M. & Hennig, J. 1998 The processing of first- and second-order motion in human visual cortex assessed by functional magnetic resonance imaging (fMRI). *J. Neurosci.* **18**, 3816–3830.

Sobey, P. & Srinivasan, M. V. 1991 Measurement of optical flow by a generalized gradient scheme. *J. Opt. Soc. Am.* A **8**, 1488–1498.

Somers, D. C., Seiffert, A. E., Dale, A. M. & Tootell, R. B. H. 1998 Second-order motion stimulus-induced activation and attentional modulation of human visual cortical areas MT & V3a. *Invest. Ophthalmol. Vis. Sci.* **39**, 1129.

Somers, D. C., Seiffert, A. E., Dale, A. M. & Tootell, R. H. 1999 fMRI investigations of motion aftereffects with lst- and 2nd-order stimuli. *Invest. Ophthalmol. Vis. Sci.* **40**, 199.

Ukkonen, O. I. & Derrington, A. M. 2000 Motion of contrast-modulated gratings as analysed by different mechanisms at low and at high contrasts. *Vis. Res.* **40**, 3359–3371.

Vaina, L. M. & Cowey, A. 1996 Impairment of the perception of second order motion but not first order motion in a patient with unilateral focal brain damage. *Proc. R. Soc. Lond.* B **263**, 1225–1232.

Vaina, L. M., Makris, N., Kennedy, D. & Cowey, A. 1998 The selective impairment of the perception of first-order

motion by unilateral cortical brain damage. *Vis. Neurosci.* **15**, 333–348.

Vaina, L. M., Cowey, A. & Kennedy, D. 1999 Perception of first- and second-order motion: separable neurological mechanisms? *Hum. Brain Mapp.* **7**, 67–77.

Van Santen, J. P. H. & Sperling, G. 1984 Temporal covariance model of human motion perception. *J. Opt. Soc. Am.* A **1**, 451–473.

Van Santen, J. P. H. & Sperling, G. 1985 Elaborated Reichardt detectors. *J. Opt. Soc. Am.* A **2**, 300–321.

Verri, A., Straforini, M. & Torre, V. 1992 Computational aspects of motion perception in natural and artificial vision systems. *Phil. Trans. R. Soc. Lond.* B **337**, 429–443.

Victor, J. D. & Conte, M. M. 1992 Evoked potential and psychophysical analysis of Fourier and non-Fourier motion mechanisms. *Vis. Neurosci.* **9**, 105–123.

Watson, A. B. & Ahumada, A. J. 1985 Model of human visual-motion sensing. *J. Opt. Soc. Am.* A **2**, 322–341.

As this paper exceeds the maximum length normally permitted, the authors have agreed to contribute to production costs.